Nanophthalmos-Associated *MYRF* Gene Mutation Causes Ciliary Zonule Defects in Mice

Xiaowei Yu, Nannan Sun, Xue Yang, Zhenni Zhao, Xiaoqian Su, Jiamin Zhang, Yuqing He, Yixiu Lin, Jian Ge, and Zhigang Fan

State Key Laboratory of Ophthalmology, Department of Glaucoma, Zhongshan Ophthalmic Center, Sun Yat-sen University, Guangzhou, Guangdong, China

Correspondence: Zhigang Fan, Jinsui Road No. 7, Zhongshan Ophthalmic Center, Sun Yat-sen University, Guangzhou, 510060, China; fanzhg3@mail.sysu.edu.cn.
Jian Ge, Jinsui Road No. 7, Zhongshan Ophthalmic Center, Sun Yat-sen University, Guangzhou, 510060, China; gejian@mail.sysu.edu.cn.

XY and NS contributed equally to this work.

Received: August 28, 2020
Accepted: February 9, 2021
Published: March 1, 2021

Citation: Yu X, Sun N, Yang X, et al. Nanophthalmos-associated *MYRF* gene mutation causes ciliary zonule defects in mice. *Invest Ophthalmol Vis Sci*. 2021;62(3):1. https://doi.org/10.1167/iovs.62.3.1

Purpose. Patients with nanophthalmos who undergo intraocular surgery often present with abnormal ciliary zonules. In a previous study, we reported mutation in *MYRF* that is implicated in the pathogenesis of nanophthalmos. The aim of this study was to model the mutation in mice to explore the role of *MYRF* on zonule structure and its major molecular composition, including *FBN1* and *FBN2*.

Methods. Human *MYRF* nanophthalmos frameshift mutation was generated in mouse using the CRISPR-Cas9 system. PCR and Sanger sequencing were used for genotype analysis of the mice model. Anterior chamber depth (ACD) was measured using hematoxylin and eosin–stained histology samples. Morphologic analysis of ciliary zonules was carried out using silver staining and immunofluorescence. Transcript and protein expression levels of *MYRF*, *FBN1*, and *FBN2* in ciliary bodies were quantified using quantitative real-time PCR (qRT-PCR) and Western blot.

Results. A nanophthalmos frameshift mutation (c.789delC, p.N264fs) of *MYRF* in mice showed ocular phenotypes similar to those reported in patients with nanophthalmos. ACD was reduced in *MYRF* mutant mice ($MYRF^{mut/+}$) compared with that in littermate control mice ($MYRF^{+/+}$). In addition, the morphology of ciliary zonules showed reduced zonular fiber density and detectable structural dehiscence of zonular fibers. Furthermore, qRT-PCR analysis and Western blot showed a significant decrease in mRNA expression levels of *MYRF*, *FBN1*, and *FBN2* in $MYRF^{mut/+}$ mice.

Conclusions. Changes in the structure and major molecular composition of ciliary zonules accompanied with shallowing anterior chamber were detected in $MYRF^{mut/+}$ mice. Therefore, *MYRF* mutant mice strain is a useful model for exploring pathogenesis of zonulopathy, which is almost elusive for basic researches due to lack of appropriate animal models.

Keywords: nanophthalmos, *MYRF* mutant mice, ciliary zonules, silver staining

Several eye disorders present with a reduced eye size, including microphthalmia, anterior microphthalmos, posterior microphthalmos, and nanophthalmos. Nanophthalmos is mainly characterized by a short axial length (AL; less than 20 mm) accompanied with small corneal diameter, shallow anterior chamber, anomalies of the vein plexus, and thick choroid and sclera, but it appears morphologically normal.[1] These anatomic characteristics present higher risk for secondary pathologies, including angle-closure glaucoma, ciliary zonule defects, and retinal folds.[2,3] Moreover, risk of complications, such as aqueous misdirection, retinal detachment, vitreous hemorrhage, and choroidal effusion, increases significantly during intraocular surgery or postoperatively in patients with nanophthalmos.[2,4] Therefore, pathologic mechanisms of nanophthalmos should be explored to provide scientific understanding of this complex condition and form a basis for improving current surgical strategies, thus achieving better prognosis for the patients.

From a molecular perspective, the mechanisms of nanophthalmos corresponding to its anatomic features include abnormal regulation in AL; anterior chamber angle–related structure configurations, including lenses and ciliary zonules; and anomaly in retina-choroid-sclera complex. Previous genetic studies report that most genes associated with nanophthalmos play a role in the development of these ocular structures. Transmembrane protein 98 (*TMEM98*, OMIM 615949),[3,5] crumbs homolog 1 (*CRB1*, OMIM 604210),[6] and bestrophin 1 (*BEST1*, OMIM 607854)[7] are implicated in the retina-choroid-sclera complex. Further, membrane-type frizzled-related protein (*MFRP*, OMIM 606227)[8] and serine protease 56 (*PRSS56*, OMIM 613858)[9] are implicated in the regulation of AL. However, currently no studies have explored the relationship of nanophthalmos-associated genes with anterior segment anatomy, specifically ciliary zonules, which is related to zonulopathy and narrowing of anterior chamber angle. Understanding the molecular mechanisms of zonulopathy and narrowing of anterior chamber angle in patients with nanophthalmos will provide information on primary angle-closure glaucoma (PACG) associated clinical phenotypes. In addition, zonu-

lopathy is common in patients with nanophthalmos and is a significant risk factor for intraocular surgery complications. Therefore, the aim of this study was to explore the structure and main molecular components of zonules in nanophthalmos gene mutations.

In a previous study, we have reported that the *MYRF* gene is implicated in the pathogenesis of nanophthalmos using a de novo mutation (DNM) strategy by trio-based whole-genome sequencing (WGS). Two DNMs of MYRF (c.789delC, p.S264fs and c.789dupC, p.S264fs) were detected in the probands of 11 trios.[10] Myelin-gene regulatory factor (*MYRF*) is a key transcriptional regulator for oligodendrocyte maturation and central nervous system myelination.[11] Furthermore, haploinsufficiency of *MYRF* results in a genetic syndrome characterized by congenital heart defects, urogenital anomalies, congenital diaphragmatic hernia, and pulmonary hypoplasia.[12] In addition, Garnai et al.[13] report that *MYRF* is important for development of the retinal pigment epithelium (RPE) and retina by the generation of *MYRF* conditional knockout mice. Moreover, truncation mutations in the C-terminal region of *MYRF* has been reported in high hyperopia families, and knockdown of *MYRF* results in small eye size in zebrafish.[13,14] However, the exact role of *MYRF* in eyes should be explored further. Therefore, in this study, we modeled human nanophthalmos frameshift mutations in mice to explore the role of *MYRF* in ciliary zonule structure and its major molecular composition, including fibrillin 1 (*FBN1*) and fibrillin 2 (*FBN2*), through immunofluorescent staining, quantitative real-time PCR (qRT-PCR) analysis and Western blot. Significantly, silver staining was used to evaluate the fine structure of zonules for the first time.

Methods

Mice

C57BL/6J mice were purchased from Beijing Biocytogen Co., Ltd. (Beijing, China). All animal procedures were conducted according to protocols approved by the Institutional Animal Care and Use Committee in the Zhongshan Ophthalmic Center and strictly complied with the ARVO Statement for the Use of Animals in Ophthalmic and Vision Research. All mice were housed in an assessment pathogen-free animal facility on a 12-hour light/dark cycle during the experiments. Animals were maintained under controlled temperature (18–29°C) and humidity (40%–70%) with food and water available ad libitum.

Screening of Single-Guide RNAs

The primary RNA transcript of *MYRF* in ensemble is ENSMUST00000189897.1. For *MYRF* targeting, six single-guide RNAs (sgRNAs) were designed to target a region upstream or downstream of exon 6 (Supplementary Table S1). Accurate target sequence of CRISPR sgRNA was designed using the Optimized CRISPR Design tool (http://crispr.mit.edu). CRISPR sgRNAs were screened for on-target activity using the UCA kit (Beijing Biocytogen Co., Ltd.), and finally sgRNA 6 was chosen as it was the most active sgRNA.

Production of Cas9 mRNA and sgRNAs

Cas9 mRNA and sgRNAs were transcribed with T7 RNA polymerase in vitro. T7 promoter sequence was added to the Cas9 and sgRNA templates by PCR amplification for Cas9 mRNA and sgRNA production. T7-Cas9 and T7-sgRNA PCR products were gel purified and used as the template for in vitro transcription with the mMESSAGE mMACHINE kit and MEGAshortscript T7 kit (Life Technologies, Carlsbad, CA, USA), respectively following the manufacturers' protocol. Cas9 mRNA and sgRNA were purified using the MEGAclear kit and eluted with RNase-free water. The targeting oligo had one nucleotide deletion (c. 789del) and two homology arms of ~60 bp, which were used as templates to repair the double-strand breaks generated by Cas9.

Microinjection

C57BL/6 female mice (3–4 weeks old) were used as embryo donors and pseudopregnant foster mothers. Superovulated fertilized eggs were isolated from female C57BL/6J mice treated with 30 IU pregnant mare serum gonadotropin (Sigma-Aldrich, St. Louis, MO, USA) and 100 IU human chorionic gonadotropin (Sigma-Aldrich) at intervals of 50 hours. The mixtures containing Cas9 mRNA (50 ng/μL), sgRNA (100 ng/μL), and oligo donor were then co-microinjected into the cytoplasm of zygotes, and surviving zygotes were transplanted into the oviducts of pseudopregnant female mice to generate live animals.

Genotyping of *MYRF*$^{mut/+}$ Mice

PCR and Sanger sequencing were used to analyze the genotype of *MYRF*$^{mut/+}$ mice. Total genomic DNA was extracted from mouse tails and then dissolved following the protocol of genomic DNA extraction kit (Tiangen, Beijing, China) for PCR and Sanger sequencing analysis. Forward primer and reverse primer sequences used for PCR are shown in Supplementary Table S2.

Histology and Anterior Chamber Depth Measurement

Mice at 4, 8, and 20 weeks old were deep-anesthetized by carbon dioxide inhalation, followed by cervical dislocation. Eyes were harvested and immediately fixed in FAS fixed liquid (Wuhan Servicebio Technology Co., Ltd., Wuhan, China) for 24 hours at 4°C. Eyeballs were then transferred to ethanol for paraffin embedding after dehydration. After embedding, samples were cut into 5-μm-thick sections through the optic nerve head. Sections were stained with hematoxylin and eosin (HE) using standard protocols. Ocular anterior segments were then examined under a light microscope DMi8 (Laica, Wetzlar, Germany) and images obtained. Anterior chamber depth (ACD) was measured as the distance from the corneal endothelium to the anterior lenticular surface centered over the pupil. AL measurements were taken from the base of the optic nerve to the center of the cornea, whereas lens thickness (LT) was measured as the distance between anterior and posterior surface of lens. Simple crowding value (calculated as (LT − ACD)/AL) was used to evaluate the crowding condition of the eye.[15]

Silver Staining

Various tissue staining techniques, including HE staining and oxytalan staining (aldehyde-fuchsin staining), were repeatedly tested for visualizing and quantifying ciliary zonules. Silver staining was the most effective technique for

Investigative Ophthalmology & Visual Science

quantifying major zonular fibrils between ciliary body and lens. Eyes in paraffin embedding were cut into 10-µm-thick sections through the optic nerve head. After dewaxing with xylene and dehydrating samples with gradient ethanol, sections were fixed using fixative solution (50% methanol, 10% acidic acid, 50 µL formaldehyde/100 mL solution) for 1 hour to overnight. Fixed sections were then treated for 1 minute with hypo solution (sodium thiosulfate solution 20 mg/100 mL) and washed with distillation-distillation H_2O three times (5 minutes each). Sections were stained with silver nitrite solution (200 mg/100 mL) for 30 minutes, developed in 100 mL developing solution (6 g sodium carbonate, 2 mL hypo solution, 50 µL formaldehyde) for 10 minutes and stopped with 5% acidic acid. Images focused on ciliary zonules were then obtained using LSM710 laser scanning confocal microscope (ZEISS, Jena, Germany). Five *MYRF*$^{mut/+}$ mice and 5 *MYRF*$^{+/+}$ mice were randomly selected and used for quantification of major zonular fibrils. One eye from each mouse was cut into paraffin sections through the optic nerve head and then silver staining performed. Major zonular fibrils in two fields (right and left fields) of each section were counted and the average major zonular fibrils number of two fields was recorded as the major zonular fibrils number of the section.

Immunohistochemistry

After dewaxing with xylene and dehydrating sections with gradient ethanol, they were placed into citrate buffer (0.01 mol/L, pH 6.0) and heated in boiling water for 30 minutes to repair antigenic ability. Sections were then washed twice with PBS at room temperature for 10 minutes and incubated with blocking solution (5% normal goat serum in PBS) at room temperature for 1 hour. Further, sections were incubated with primary antibodies, including rabbit anti-MYRF (bs-11191R, 1:500; Biosynthesis Biotechnology Co., Ltd., Beijing, China), rabbit anti–fibrillin 1 (ab53076, 1:200; Abcam, Cambridge, MA, USA), and mouse anti–fibrillin 2 (sc-393968, 1:200; Santa Cruz Biotechnology, Santa Cruz, CA, USA), separately overnight at 4°C. Samples were then washed with PBS and incubated with Alexa Fluor 488–conjugated donkey anti-rabbit secondary antibody (A21206, 1:800; Invitrogen, Carlsbad, CA, USA) or Alexa Fluor 594–conjugated donkey anti-mouse secondary antibody (A11058, 1:800; Invitrogen) for 2 hours at room temperature. Samples were then counterstained with 4, 6-diamidino-2-phenylindole (Biofroxx GmbH, Germany) and washed with PBS. Immunofluorescence images focused on ciliary zonules were then obtained using the LSM710 laser-scanning confocal microscope (ZEISS).

Tissue Collection, RNA Isolation, and Quantitative Real-Time PCR Analysis

Mice were euthanized and ciliary bodies were harvested directly under a stereoscopic microscope. A small hole was made using a syringe needle, and a small incision was made in the cornea. The posterior portion of the globe, including sclera, choroid, and retina, was dissected to the level of the pars plana and discarded. The iris was then isolated completely from the iris–ciliary body complex as much as possible, and finally the ciliary body was dissociated carefully from the sclera and lens using micro-forceps. Total RNA was extracted from the ciliary body with TRIzol (TaKaRa, Dalian, China) following the manufacturer's instruction. Purified total RNA was quantified using a Nanodrop-1000 spectrophotometer (Thermo Fisher Scientific, Carlsbad, CA, USA). RNA was reverse-transcribed into cDNA using the First-Strand cDNA Synthesis Kit (Applied Biological Materials [ABM], Inc., Richmond, BC, Canada). qRT-PCR was performed using the SYBR Green Master Mix (Roche Life Science, Basel, Switzerland) in the Roche LightCycler 384. Primer sequences used are summarized in Supplementary Table S2.

Western Blot Analysis

Ciliary bodies were immediately frozen in liquid nitrogen after dissecting them from eyes. Each sample was then lysed in 100 µL ice-cold RIPA buffer (Fude Biological Technology Co., Ltd., Hangzhou, China) supplemented with protease inhibitors and sonicated. Homogenates were centrifuged at 12,000 × *g* at 4°C for 5 minutes. Supernatants were collected and mixed with 6× loading buffer (Fude Biological Technology Co., Ltd.). After protein denaturation at 95°C for 5 minutes, samples were subjected to electrophoresis with 12% SDS-PAGE and electroblotted to polyvinylidene fluoride membranes (Millipore, Billerica, MA, USA). Membranes were blocked with 5% skim milk at room temperature for 2 hours and then incubated with primary antibodies: rabbit anti-MYRF (bs-11191R, 1:2000; Biosynthesis Biotechnology Co., Ltd.), rabbit anti–fibrillin 1 (ab53076, 1:2000; Abcam), and mouse anti–fibrillin 2 (sc-393968, 1:2000; Santa Cruz Biotechnology, Inc.) overnight at 4°C. After washing three times for 10 minutes with TBST, membranes were incubated with goat anti-mouse horseradish peroxidase (HRP)-conjugated secondary antibody (1:5000; Thermo Fisher Scientific, Carlsbad, CA, USA) or goat anti-rabbit HRP-conjugated secondary antibody (1:5000; Thermo) at room temperature for 2 hours, followed by washing with TBST for three times. Membranes were then scanned using the MP ChemiDoc Imaging System (Bio-Rad, Berkeley, California, USA). ImageJ software (National Institutes of Health, Bethesda, MD, USA) was used to analyze densitometric values of Western blot bands.

Statistical Analysis

All data are presented as mean ± SEM. Comparisons of two individual experimental groups were performed using Student's *t*-test or the Mann-Whitney *U*-test based on the distribution of the data. SPSS 20.0 software (SPSS, Chicago, IL, USA) and GraphPad Prism 6 (version 6.01; GraphPad Software, La Jolla, CA, USA) were used for statistical analysis and generation of figures. $P < 0.05$ was considered statistically significant.

Results

Generation of *MYRF*$^{mut/+}$ Mice With CRISPR/Cas9 Genetic Editing System

To explore the effect of a human nanophthalmos frameshift mutation in *MYRF* on ciliary zonules, we successfully established *MYRF*$^{mut/+}$ mice in the C57BL/6J mouse strain. Exon 6 was scanned for sgRNA target sequence design to delete a cytosine deoxyribonucleotide causing frameshift mutation (c.789del, p.N264fs) (Fig. 1A). *MYRF*$^{mut/+}$ founders (F0) were generated by co-microinjection of the cocktail of Cas9

Investigative Ophthalmology & Visual Science

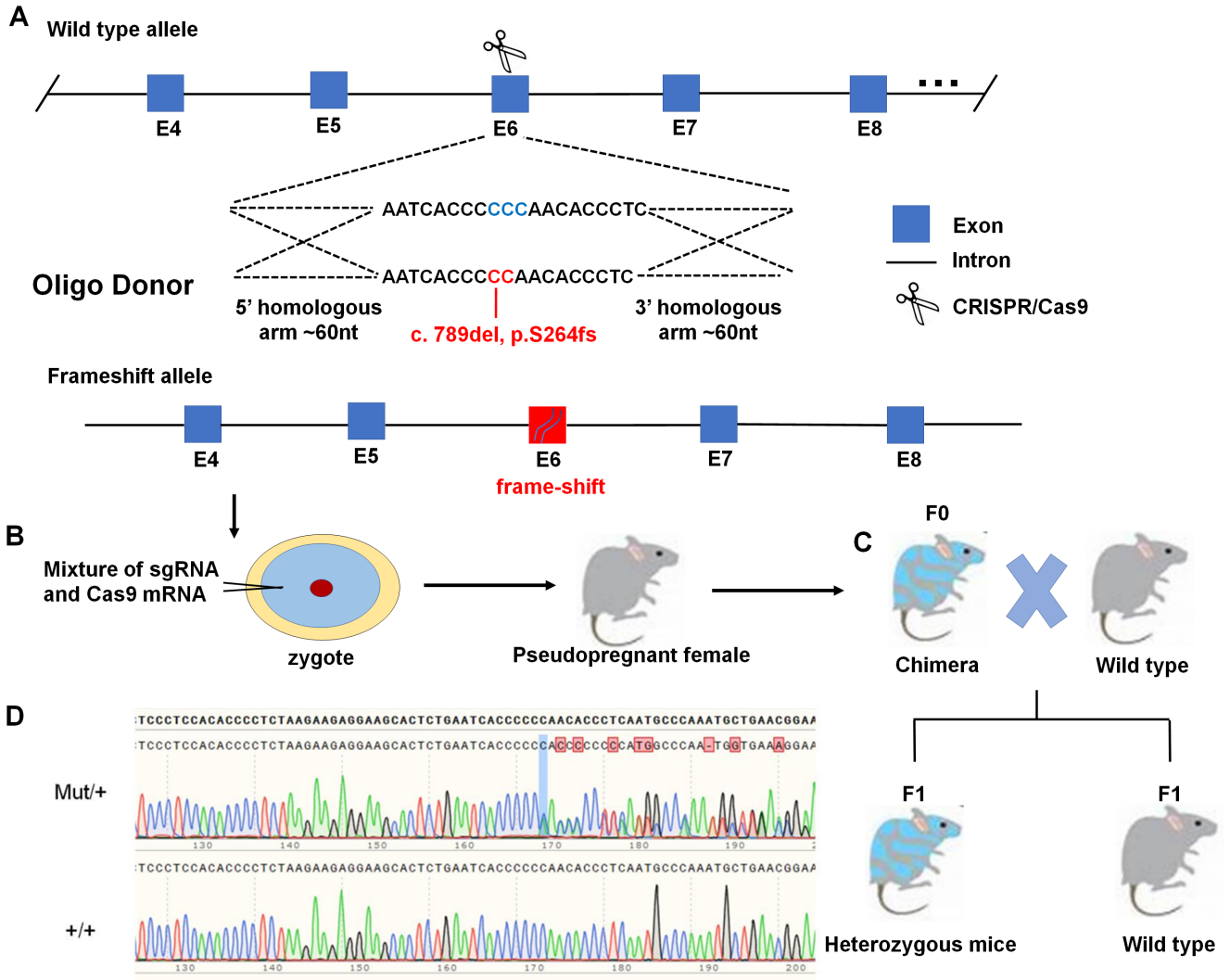

Figure 1. Generation of *MYRF*$^{mut/+}$ mice using the CRISPR/Cas9 system. (**A**) Schematic diagram of the *MYRF* gene encoding deoxyuridine 5′-triphosphate nucleotidohydrolase (dUTPase). Exons are indicated with *blue rectangles* and marked with *E* and numbers while introns are indicated with the *short black line*. Guide RNA (gRNA) target sites and protospacer adjacent motif (PAM) sequence are *underlined* in *blue* and *red*, respectively. (**B**) Embryonic stem (ES) cell was microinjected with sgRNA and Cas9 mRNA and matured as a blastocyst, which was subsequently transferred to pseudo-pregnant female mice. (**C**) The chimeras (F0) were crossbred with wild-type mice to generate littermate control mice (*MYRF*$^{+/+}$) and heterozygous (*MYRF*$^{mut/+}$) offspring (F1) containing the targeted locus through germline transmission. (**D**) Base sequence in *MYRF*$^{mut/+}$ and *MYRF*$^{+/+}$.

mRNA, sgRNA, and oligo donor into the cytoplasm of zygotes (Fig. 1B). Founder (F0) mice with targeted *MYRF* mutation were validated by PCR and Sanger sequencing analysis (Fig. 1D). In case of the rapid cleavage in the early embryonic stage, F0 mice would be mosaic. Therefore, three heterozygous mice (F1 mice) with heritable genotype were obtained after verifying that the targeted deoxyribonucleotide in exon 6 was mutated. Subsequently, F1 mice were intercrossed with C57BL/6J wild-type mice to generate more F2 heterozygous offspring for subsequent experiments (Fig. 1C). In addition, we have tried to generate homozygote offspring through hybridization between heterozygotes. However, no live *MYRF* homozygote mutation mice were obtained because homozygote *MYRF* gene mutation led to premature death during the embryonic period, and the offspring of heterozygotes had normal Mendelian segregation ratios (19 *MYRF*$^{mut/+}$ mice vs. 8 *MYRF*$^{+/+}$ mice, χ^2 P = 0.683). Heterozygous offspring with the same targeted *MYRF* mutation were verified by PCR and Sanger sequencing analysis. All the *MYRF* mutation mice used in our experiments had the same targeted mutation. Weight, growth, and behavior of *MYRF*$^{mut/+}$ mice were normal.

mRNA and Protein Expression Levels of *MYRF* Decreased in *MYRF*$^{mut/+}$ Mice Ciliary Bodies

To determine *MYRF* expression pattern in ocular tissues, immunohistochemistry was carried out on the whole mice eyeball. Relative high expression level of *MYRF* was observed in the ciliary body and retina, including RPE, inner nuclear layer (INL), and ganglion cell layer (GCL) (Fig. 2). In addition, a similar pattern of *MYRF* mRNA expression was observed in human ocular tissues. RPE showed the highest expression level of *MYRF* mRNA followed by the ciliary

Investigative Ophthalmology & Visual Science

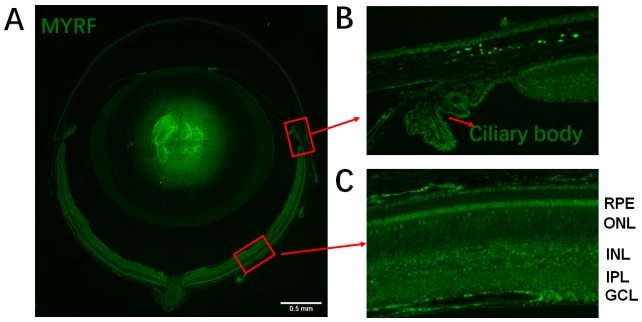

Figure 2. *MYRF* expression pattern in mice ocular tissues. (**A**) Eyeball panorama gram of *MYRF* immunofluorescence. *Scale bar*: 0.5 mm. (**B**) Partial enlarged detail of anterior chamber structures shows the high *MYRF* expression in the ciliary body. (**C**) Partial enlarged detail of retina shows the high *MYRF* expression in RPE, INL, and GCL.

body and retina.[13] To quantify expression of *MYRF* at the transcript and protein level in $MYRF^{mut/+}$ mice ciliary bodies, quantitative real-time PCR and Western blot of ciliary bodies were performed. A significant decrease in *MYRF* mRNA and protein expression was observed in $MYRF^{mut/+}$ mice ciliary bodies compared with expression levels in $MYRF^{+/+}$ mice ($P < 0.01$, Figs. 5, 6).

Human Nanophthalmos Frameshift Mutation of *MYRF* in Mice Results in a Shallow Anterior Chamber Depth

A shallow anterior chamber is an important characteristic of nanophthalmos in humans. To investigate the effect of *MYRF* mutation on mice ocular anterior segments, HE staining was used to measure ACD (from the corneal endothelium to the anterior lenticular surface, centered over the pupil) and AL of total six littermate control mice ($MYRF^{+/+}$) and six mutant mice ($MYRF^{mut/+}$) (Fig. 3A). Mean ACDs of $MYRF^{+/+}$ mice and $MYRF^{mut/+}$ mice were 0.43 ± 0.04 and 0.37 ± 0.005 mm, respectively ($P < 0.01$, Fig. 3B). This finding implies that the ACD of $MYRF^{mut/+}$ mice was significantly reduced compared with the ACD of the control group. In addition, we analyzed ACD and AL ratio and simple crowding value of these mice. The mean ACD/AL was significantly higher in $MYRF^{+/+}$ mice (0.14) compared with the ACD/AL in $MYRF^{mut/+}$ mice (0.12) ($P < 0.01$). Simple crowding was significantly lower in $MYRF^{+/+}$ mice (0.44) compared with simple crowding in $MYRF^{mut/+}$ mice (0.48) ($P < 0.001$). Significantly higher simple crowding value in $MYRF^{mut/+}$ mice implies a crowding condition of the eye. However, the mean AL in $MYRF^{mut/+}$ mice was not significantly different compared with the mean AL of $MYRF^{+/+}$ mice (Supplementary Fig. S1).

The patient with frameshift mutation (c.789delC, p.S264fs) was a 16-year-old girl with bilaterally short AL (OD: 18.09 mm; OS: 18.07 mm).[10] Notably, she was diagnosed with secondary angle-closure glaucoma after a visit to our facility. Ultrasound Biomicroscopy (UBM) analysis showed that her ACD was 2.68 mm OD and 2.37 mm OS, which implies that the abnormal ciliary zonule and lens states as lens dislocation were characterized by binocular asymmetry of anterior chamber depth.[16] Mice used for ACD and AL measurement were 8 weeks old (young adults), which matched with the disease onset in this patient. In addition, reduced ACD was reported from postnatal 4 weeks and did not progress significantly until postnatal 20 weeks (Fig. 3C). Therefore, 8-week-old mice (young adults) were used for all subsequent experiments.

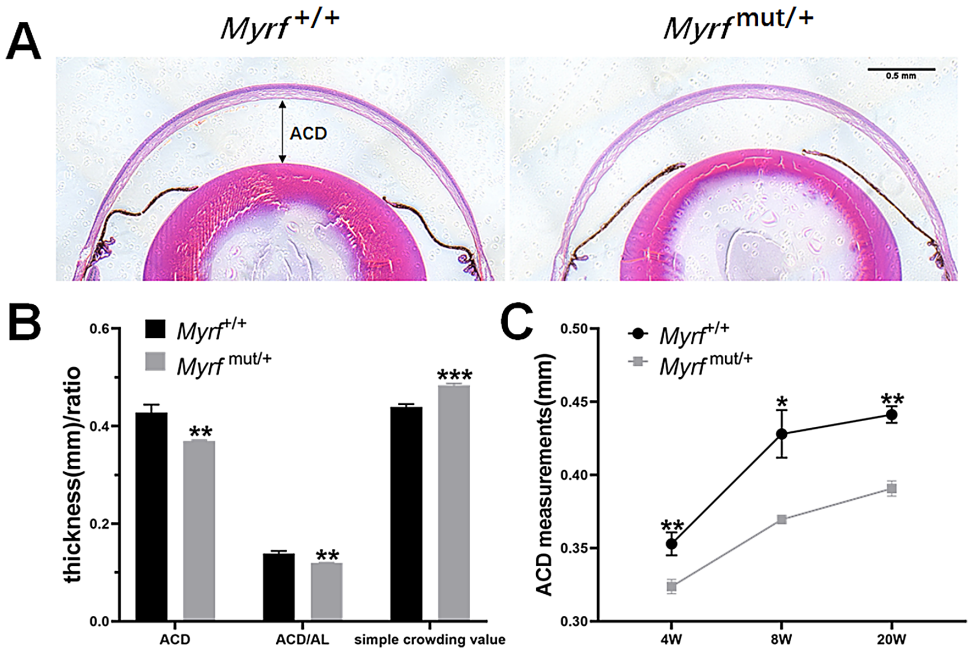

Figure 3. Reduced anterior chamber depth in $MYRF^{mut/+}$ mice. (**A**) Representative HE staining images of midsagittal sections of mouse eyes showed a difference in ACD between $MYRF^{mut/+}$ mice and $MYRF^{+/+}$ mice. *Scale bar*: 50 µm. (B) The mean ACD, ACD/AL ratio, and simple crowding value in $MYRF^{mut/+}$ mice and $MYRF^{+/+}$ mice. (**C**) ACD measurements at 4, 8, and 20 weeks old in $MYRF^{mut/+}$ mice and $MYRF^{+/+}$ mice. Data represent mean ± SEM. $n = 6$. *$P < 0.05$, **$P < 0.01$, ***$P < 0.001$ versus $MYRF^{+/+}$ mice.

Investigative Ophthalmology & Visual Science

Ciliary Zonule Defects Were Present in *MYRF*$^{mut/+}$ Mice as Demonstrated by Silver Staining and Immunofluorescence

Ciliary zonules are made of fibrillin microfibril bundles and play an important role in anchoring the eye lens to the ciliary body.[17] Clinically, zonule defects are usually secondary to nanophthalmos and are associated with shallow ACD and crowding condition of ocular anterior segments. Therefore, we focused on phenotypes related to ciliary zonule defects in *MYRF*$^{mut/+}$ mice. For the first time, we tested and adopted silver staining strategy to explore the delicate structure of ciliary zonules. The density of zonular fibers extending from the ciliary epithelium to the lens equator was reduced, and the zonule morphology was altered in *MYRF*$^{mut/+}$ mice (Fig. 4B). On the contrary, the fibrous structure of ciliary zonules remained intact in *MYRF*$^{+/+}$ mice (Fig. 4B). After performing silver staining, several zonular fibers were identified (shown with asterisks in Fig. 4B), which were defined as major zonular fibrils to quantify the change of zonular fibers. Further quantification showed that the mean number of major zonular fibrils was significantly decreased ($P < 0.05$, Fig. 4D), indicating that structural defects of ciliary zonules occurred in nanophthalmos-associated *MYRF* mutants. *FBN1* and *FBN2* are the most important molecular markers of fibrillin microfibrils in zonules.[18] Therefore, an immunofluorescence technique was used to stain eye samples with respective antibodies. Immunofluorescent analysis showed that both major *FBN1*-stained and *FBN2*-stained fibers were reduced in *MYRF*$^{mut/+}$ zonules compared with those in *MYRF*$^{+/+}$ zonules ($P < 0.01$, Figs. 4C, 4E, 4F), which was consistent results obtained with silver staining.

mRNA Expression of Both *FBN1* and *FBN2* was Decreased in *MYRF*$^{mut/+}$ Mice

Fibrillins, the major components of mouse zonules similar to those in humans, are mainly derived from nonpigmented ciliary epithelium (NPCE). *FBN1* and *FBN2* encoding abundant zonular proteins are expressed predominantly in the NPCE throughout development.[18] Therefore, we dissected ciliary bodies to analyze expression levels of both *FBN1* and *FBN2* by qRT-PCR analysis and Western blot. The results showed a significant decrease in mRNA and protein expression levels of *FBN1* and *FBN2* in *MYRF*$^{mut/+}$ mice ($P < 0.05$, Figs. 5, 6). These results imply that production of fibrillins from NPCE was reduced in *MYRF*$^{mut/+}$ mutants, which is consistent with the phenotype of zonule defects.

Discussion

In a previous study, we reported a mutation in *MYRF* (c.789delC, p.S264fs), which is a gene implicated in nanophthalmos through trio-based WGS analysis.[10] Therefore, in this study, we modeled the mutation in mice to explore the role of *MYRF* in ciliary zonule structure and its major molecular composition.

At first, we performed immunofluorescence analysis to evaluate the *MYRF* expression pattern in mice. Results showed significantly high expression levels of *MYRF* in ciliary bodies and retina, including RPE, INL, and GCL. A similar pattern of *MYRF* mRNA expression is reported in human ocular tissues, with the highest expression level recorded in RPE and relatively high expression level in ciliary bodies and retina.[13] Therefore, further studies should explore the role of *MYRF* in RPE, retina, and ciliary bodies. However, significant abnormal nanophthalmos-related ocular phenotypes, including short AL, retinal folds, RPE defeats, high intraocular pressure, and thinner retinal nerve fiber layer or significant abnormal nonocular phenotypes found in *MYRF* Olig2 conditional knockout mice, including tremors, ataxia, and seizures,[11] were not observed (data not shown). Instead, ciliary zonule defects accompanied with a shallow ACD, decreased ACD/AL ratio, and increased simple crowding value were observed in *MYRF*$^{mut/+}$ mice. These findings imply that *MYRF* is important for integrity of ciliary zonules. Analysis of silver staining results showed that the morphology of ciliary zonules was altered with reduced zonular fiber density and significant structural dehiscence in zonular fibers in *MYRF*$^{mut/+}$ mice compared with the features in the control group. The principal structural component of the ciliary zonule is fibrillin, a cysteine-rich glycoprotein. Three fibrillin isoforms (FBN1–3) are present in humans, whereas the gene *FBN3* is inactive in mouse.[19] Therefore, the profile *FBN1* and *FBN2* in *MYRF*$^{mut/+}$ mice was evaluated to determine if *MYRF* deficiency affects the principal structural component of the ciliary zonule. Immunofluorescent analysis showed that *FBN1* staining and *FBN2* staining were reduced in *MYRF*$^{mut/+}$ zonules. Furthermore, mRNA and protein expression of *MYRF*, *FBN1*, and *FBN2* in ciliary bodies was downregulated in mutant mice.

Low expression level of *MYRF* at the transcript and protein level in *MYRF*$^{mut/+}$ mice can be attributed to two reasons. First, after the frameshift mutation, the termination codon appeared in advance at the amino acid position 271, resulting in a truncated protein (length of 270). The premature termination codon might trigger the nonsense-mediated mRNA decay (NMD) pathway, resulting in *MYRF* mRNA degradation. Second, the truncated protein might not trigger the NMD pathway, whereas the shorter *MYRF* fragment resulted in decreased transcript and protein expression of *MYRF*. Whatever the actual mechanism was, *MYRF* transcript and protein expression levels were lower in *MYRF*$^{mut/+}$ mice ciliary bodies, implying that *MYRF* plays an important role in zonular defects. On the other hand, we could not exclude the possibility that the *MYRF* truncated protein may act in a dominant-negative manner, resulting in the observed phenotype. The underlying mechanism of zonular defects caused by *MYRF* frameshift mutation should be further investigated.

Several nanophthalmos-associated gene mutation mouse models have been used to investigate the human nanophthalmos phenotype. Neither *Mfrp* knockout mice nor *Tmem98* mutation mice showed a statistically significant reduction in AL measurements.[3,20] Similarly, our findings on *MYRF*$^{mut/+}$ mice showed that AL was slightly reduced, but the decrease was not statistically significant. Although there is a measurable difference in ACD, AL may not change significantly due to the relatively minor proportion of ACD in AL. Additionally, mouse eyes are very small, which may require novel and more precise methods to achieve biologically meaningful accuracy. Use of the HE-stained section to measure AL does not accurately simulate the condition of a living eye, because intraocular pressure change after dehydration may result in measurement bias. The ACD structure is relatively more stable compared with the overall AL in an eyeball; therefore, measurement of ACD using HE staining is more accurate in demonstrating the phenotype of *MYRF*$^{mut/+}$ mice. Therefore, spectral-domain

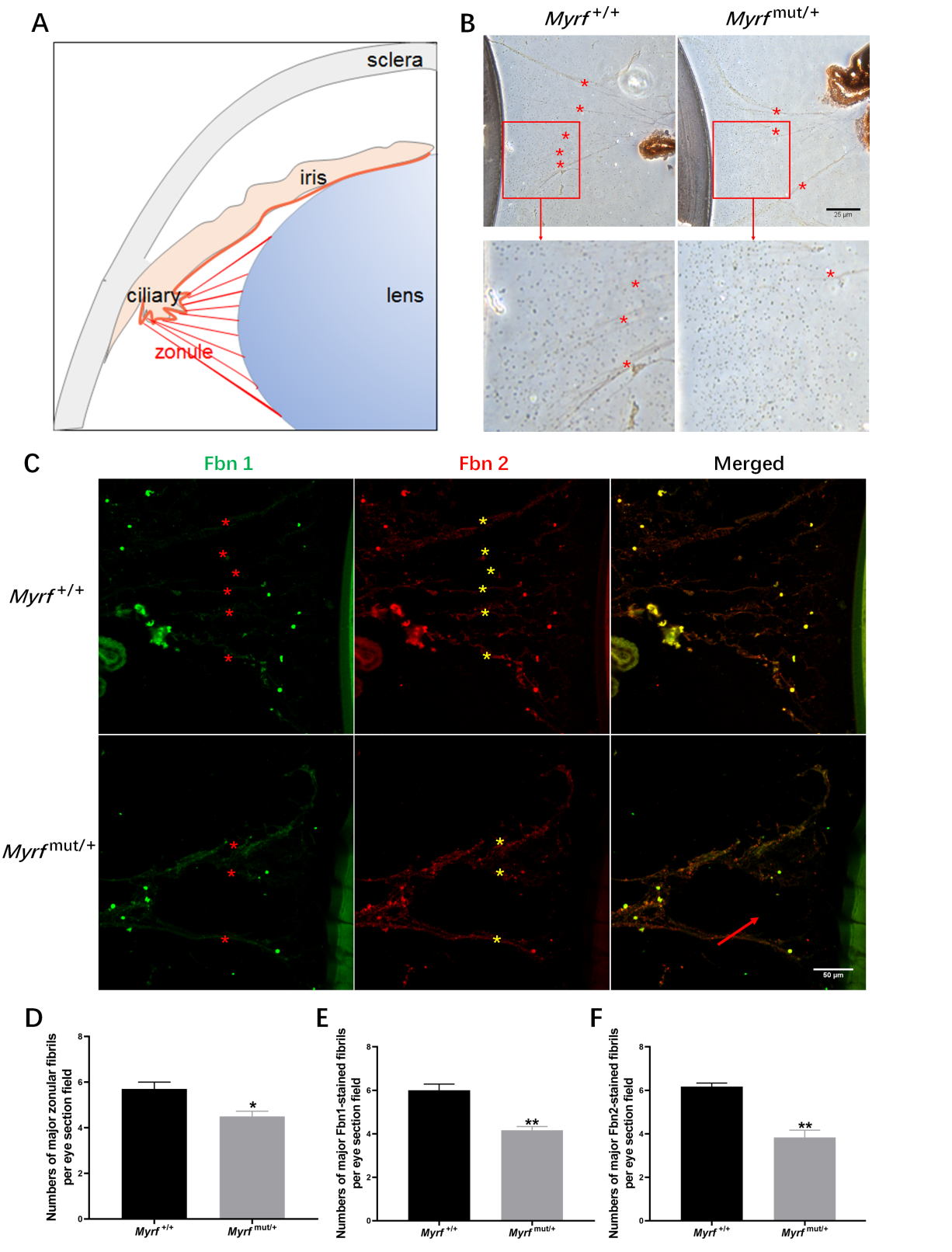

Figure 4. Ciliary zonule defects in $MYRF^{mut/+}$ mice. (**A**) Pattern of anterior angle structures. (**B**) Silver staining demonstrated reduced zonular fibers density and zonular fibers dehiscence in $MYRF^{mut/+}$ mice compared to those in $MYRF^{+/+}$ mice. Major zonular fibers were labeled with *asterisks*. *Scale bar*: 25 µm. (**C**) Immunofluorescence analysis showed that fluorescence intensity of both *FBN1* and *FBN2* staining was significantly reduced in the zonules of $MYRF^{mut/+}$ mice compared with those in $MYRF^{+/+}$ controls. The deficiency of *FBN1* and *FBN2* staining was labeled with *red arrows*. Major zonular fibers were labeled with *asterisks*. *Scale bar*: 50 µm. (**D**) Quantification of the number of major zonule fibers per eye section field in $MYRF^{mut/+}$ and $MYRF^{+/+}$ mice. The mean value was 5.7 ± 0.6 in $MYRF^{+/+}$ mice and 4.5 ± 0.4 in $MYRF^{mut/+}$ mice. Data represent mean ± SEM. $n = 5$. $^{*}P < 0.05$ versus $MYRF^{+/+}$ mice. (**E**, **F**) Quantification of the number of major *FBN1*- and *FBN2*-stained fibers per eye section field in $MYRF^{mut/+}$ and $MYRF^{+/+}$ mice. Data represent mean ± SEM. $n = 3$. $^{**}P < 0.01$ versus $MYRF^{+/+}$ mice.

Investigative Ophthalmology & Visual Science

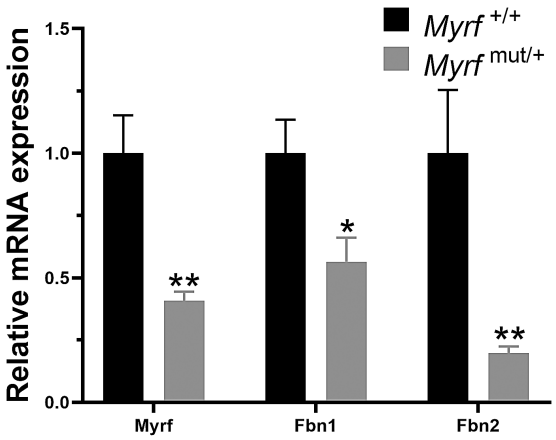

Figure 5. Transcript expression in the ciliary body. A significant decrease of *MYRF*, *FBN1*, and *FBN2* mRNA expression was shown in the $MYRF^{mut/+}$ mice ciliary body. Data represent mean ± SEM. $n = 8$. $^{*}P < 0.05$, $^{**}P < 0.01$ versus $MYRF^{+/+}$ mice.

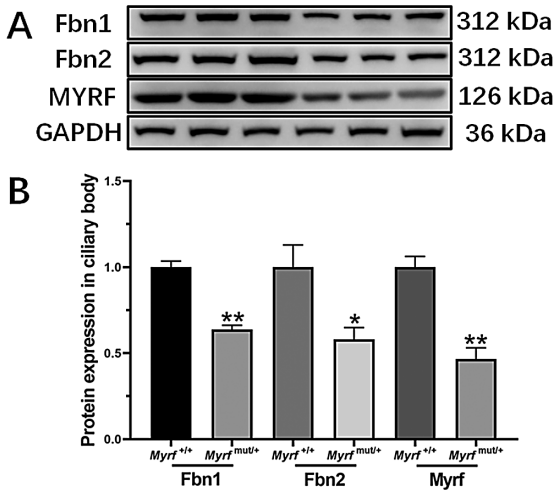

Figure 6. Protein expression in the ciliary body. Western blots showed a decrease of *MYRF*, *FBN1*, and *FBN2* protein expression in the $MYRF^{mut/+}$ mice ciliary body. $n = 3$. $^{*}P < 0.05$, $^{**}P < 0.01$ versus $MYRF^{+/+}$ mice.

optical coherence tomography with higher imaging speed and higher resolution is a better choice to measure the dimension of mouse eyes in future research.[21] On the other hand, the development of AL may be a consequence of polygenetic regulation; therefore, a single gene mutation may not be sufficient to cause significant change in AL development.

Nanophthalmos[22] is a rare ocular disorder, attributed to developmental arrest of eyes in the early stages of embryogenesis. Short AL, narrow iridocorneal angle, and shallow anterior chamber are associated with several clinical complications, with secondary angle-closure glaucoma being the most common complication.[2,23] Unlike primary angle-closure glaucoma, traditional laser peripheral iridotomy and trabeculectomy do not completely relieve high intraocular pressure in nanophthalmos, and the incidence of aqueous misdirection is significantly increased.[24] One of our hypotheses is that developmental ciliary zonule defects in nanophthalmos result in forward movement of a relatively larger-sized lens, following pupillary blockage and a shallow peripheral anterior chamber. The effect of these changes results in movement of aqueous seek backward into the vitreous cavity, thus pushing the lens-iris diaphragm forward, a trait associated with aqueous misdirection. Surgical operation in such a narrow and crowded anterior chamber with increased vitreous pressure may result in the occurrence of malignant glaucoma.[25] Our findings imply that ciliary zonule defects in *MYRF* mutation mice may be associated with developmental arrest of eyes in nanophthalmos. Experimental findings and clinical observations show that ophthalmologists should pay extra attention to changing surgical details, especially ciliary zonule defects in patients with angle-closure glaucoma secondary to nanophthalmos.

Ciliary zonules are the circumferential suspensory ligaments that span the gap between the lens and adjacent ciliary bodies. The main role of zonules is to maintain the lens in the center of the visual pathway and transmit contraction forces from ciliary bodies to the lens for accommodation.[26,27] Zonules can be classified into three subgroups: anterior, equatorial, and posterior parts based on the attachment point of these fibers on the lens.[28] Reduction in tensile strength of ciliary zonules or rupture of any fibers in any subgroup can weaken traction force to the lens. In either case, the lens might become thicker and move forward or backward. This partially explains the phenotype of ciliary zonule defects in $MYRF^{mut/+}$ mice that present with a shallow anterior chamber compared with that in the control group with intact ciliary zonules. However, fiber groups that are defective were not identified due to currently available technical limits in distinguishing fine details among the three fiber subgroups as the mouse ciliary zonule fibers are too delicate. Furthermore, available techniques for studying ciliary zonules are limited. Each zonular fiber is composed of hundreds or thousands of microfibrils with long filamentous structures about 10 to 12 nm in diameter, which would not be visible with a light microscope.[29] Ciliary zonule is a type of oxytalan fiber,[30] and therefore, traditional aldehyde fuchsin and HE staining are difficult to make it clearly visible.[31] Moreover, it is difficult to achieve good views under scanning electron microscopy due to artifacts associated with reagents for fixation and/or drying of fibers.[30] To our knowledge, this is the first time that analysis of the structure of ciliary zonules by silver staining is being reported. The findings show that ciliary zonules are distinguishable, and major zonular fibrils can be quantified. These findings provide a basis for further research on ciliary zonules, which is important but obstructed by previous lack of appropriate methodology.

Fibrillin microfibrils are the main components of ciliary zonules, and proteomic analysis shows dozens of proteins in ciliary zonular fibers, with *FBN1* and *FBN2* as the main type of proteins.[17,18] Other important proteins include latent-transforming growth factor β-binding protein 2 (*LTBP-2*), microfibrillar-associated protein 2 (*MFAP-2*), disintegrin and metalloproteinase with thrombospondin motifs (*ADAMTS*), and ADAMTS-like proteins (*ADAMTSL*).[32–34] In this study, *FBN1* and *FBN2* were used to perform immunofluorescent analysis as they are the highest expressed proteins in the ciliary zonule. Reduction level in *FBN1* and *FBN2* was further confirmed at the molecular level, indicating zonule abnormality in $MYRF^{mut/+}$ mice. The relative expression levels of *FBN1* and *FBN2* in NPCE, which play a role in the synthesis of the two zonular proteins,[35] were decreased. However, the underlying molecular mechanism of zonule defects associated with the *MYRF* mutation should be explored further.

Mutations of *FBN1* and *FBN2* caused ciliary zonule defeats and lens dislocation,[29,36–38] demonstrating that *FBN1* and *FBN2* regulate structural integrity of the ciliary zonule. Other gene mutations, such as *LTBP-2*, *ADAMTSL4*, and *CTRP5*, have also been reported to cause ciliary zonule defects.[39–41] In contrast, the *MYRF* gene is not a directly related fibrillin microfibril gene. Therefore, ciliary zonule defects in $MYRF^{mut/+}$ mice may be due to the low *FBN1* and *FBN2* expression. Nonetheless, the relationship between *MYRF*, *FBN1*, and *FBN2* needs to be further investigated. Given the lack of clinical measurements to evaluate the integrity of ciliary zonules, zonule abnormalities are often not identified until intraocular surgery, rendering patients susceptible to fatal intraoperative complications such as aqueous misdirection and posterior capsule rupture.[42] By screening for gene mutations, the risk of intraocular surgery complications caused by unstable ciliary zonules can be predicted in a timely manner.

Some limitations in this study should be considered. First, CRISPR editing might have a possibility of off-target effects, yet we have taken some measures to reduce it. We have designed six sgRNAs and finally chose the most efficient and specific one to avoid the off-targets. Additionally, Cas mRNA was used for microinjection, and the short half-life mRNA would decrease the risk of continuous cutting off the target. On the other hand, the mixtures containing Cas9 mRNA, sgRNA, and oligo donor were co-microinjected into the cytoplasm of zygotes. The targeting oligo carried one nucleotide deletion (c. 789del) and two homology arms of ~60 bp, which were used as templates to repair the double-strand breaks generated by Cas9. Second, although we have identified that there was a significant decrease in the mRNA and protein expression of *FBN1* and *FBN2* in $MYRF^{mut/+}$ mice ciliary bodies, the underlying molecular mechanism of zonule defects associated with *MYRF* mutation has yet to be further investigated through RNA-seq or tandem mass tag (TMT)-based proteome profiling.

In summary, our previous findings revealed that a DNM (c.789delC, p.S264fs) in *MYRF* is associated with human nanophthalmos.[10] We found that the same frameshift mutation in *MYRF* caused a shallowing anterior chamber and ciliary zonule defects in mice, which suggests that *MYRF* plays an important role in zonule development. More important, we have utilized a silver staining strategy to detect the structure of ciliary zonules for the first time, which may contribute to progress in future investigations of ciliary zonules. Clinically, our findings indicate that ophthalmologists should pay attention to preoperative ciliary zonule assessment in patients with nanophthalmos during cataract surgery or antiglaucoma surgery to avoid severe complications.

Acknowledgments

The authors thank Beijing Biocytogen Co., Ltd. (Beijing, China) for its technical support in the CRISPR design. This study was financially supported by Guangzhou Science and Technology Plan Project (Grant 201803040020, 201903010065; Guangzhou, China), Guangdong Natural Science Foundation (Grant 2020A151501168; Guangzhou, China), and Research Funds of the State Key Laboratory of Ophthalmology (Grant PT1001022).

Disclosure: **X. Yu**, None; **N. Sun**, None; **X. Yang**, None; **Z. Zhao**, None; **X. Su**, None; **J. Zhang**, None; **Y. He**, None; **Y. Lin**, None; **J. Ge**, None; **Z. Fan**, None

References

1. O'Grady RB. Nanophthalmos. *Am J Ophthalmol*. 1971;71:1251–1253.
2. Carricondo PC, Andrade T, Prasov L, Ayres BM, Moroi SE. Nanophthalmos: a review of the clinical spectrum and genetics. *J Ophthalmol*. 2018;2018:2735465.
3. Cross SH, McKie L, Keighren M, et al. Missense mutations in the human nanophthalmos gene TMEM98 cause retinal defects in the mouse. *Invest Ophthalmol Vis Sci*. 2019;60:2875–2887.
4. Yalvac IS, Satana B, Ozkan G, Eksioglu U, Duman S. Management of glaucoma in patients with nanophthalmos. *Eye (London, England)*. 2008;22:838–843.
5. Khorram D, Choi M, Roos BR, et al. Novel TMEM98 mutations in pedigrees with autosomal dominant nanophthalmos. *Mol Vis*. 2015;21:1017–1023.
6. Paun CC, Pijl BJ, Siemiatkowska AM, et al. A novel crumbs homolog 1 mutation in a family with retinitis pigmentosa, nanophthalmos, and optic disc drusen. *Mol Vis*. 2012;18:2447–2453.
7. Toto L, Boon CJ, Di Antonio L, et al. Bestrophinopathy: a spectrum of ocular abnormalities caused by the c.614T>C mutation in the BEST1 gene. *Retina (Philadelphia, Pa)*. 2016;36:1586–1595.
8. Fogerty J, Besharse JC. 174delG mutation in mouse MFRP causes photoreceptor degeneration and RPE atrophy. *Invest Ophthalmol Vis Sci*. 2011;52:7256–7266.
9. Paylakhi S, Labelle-Dumais C, Tolman NG, et al. Muller glia-derived PRSS56 is required to sustain ocular axial growth and prevent refractive error. *PLoS Genet*. 2018;14:e1007244.
10. Guo C, Zhao Z, Chen D, et al. Detection of clinically relevant genetic variants in chinese patients with nanophthalmos by trio-based whole-genome sequencing study. *Invest Ophthalmol Vis Sci*. 2019;60:2904–2913.
11. Emery B, Agalliu D, Cahoy JD, et al. Myelin gene regulatory factor is a critical transcriptional regulator required for CNS myelination. *Cell*. 2009;138:172–185.
12. Rossetti LZ, Glinton K, Yuan B, et al. Review of the phenotypic spectrum associated with haploinsufficiency of MYRF. *Am J Med Genet A*. 2019;179:1376–1382.
13. Garnai SJ, Brinkmeier ML, Emery B, et al. Variants in myelin regulatory factor (MYRF) cause autosomal dominant and syndromic nanophthalmos in humans and retinal degeneration in mice. *PLoS Genet*. 2019;15:e1008130.
14. Xiao X, Sun W, Ouyang J, et al. Novel truncation mutations in MYRF cause autosomal dominant high hyperopia mapped to 11p12-q13.3. *Hum Genet*. 2019;138:1077–1090.
15. Niu W-R, Dong C-Q, Zhang X, Feng Y-F, Yuan F. Ocular biometric characteristics of Chinese with history of acute angle closure. *J Ophthalmol*. 2018;2018:5835791.
16. Luo L, Li M, Zhong Y, Cheng B, Liu X. Evaluation of secondary glaucoma associated with subluxated lens misdiagnosed as acute primary angle-closure glaucoma. *J Glaucoma*. 2013;22:307–310.
17. Cain SA, Morgan A, Sherratt MJ, Ball SG, Shuttleworth CA, Kielty CM. Proteomic analysis of fibrillin-rich microfibrils. *Proteomics*. 2006;6:111–122.
18. De Maria A, Wilmarth PA, David LL, Bassnett S. Proteomic analysis of the bovine and human ciliary zonule. *Invest Ophthalmol Vis Sci*. 2017;58:573–585.
19. Kielty CM. Fell-Muir lecture: fibrillin microfibrils: structural tensometers of elastic tissues? *Int J Exp Pathol*. 2017;98:172–190.
20. Velez G, Tsang SH, Tsai YT, et al. Gene therapy restores Mfrp and corrects axial eye length. *Sci Rep*. 2017;7:16151.
21. Pardue MT, Stone RA, Iuvone PM. Investigating mechanisms of myopia in mice. *Exp Eye Res*. 2013;114:96–105.

Investigative Ophthalmology & Visual Science

22. Altintaş AK, Acar MA, Yalvaç IS, Koçak I, Nurözler A, Duman S. Autosomal recessive nanophthalmos. *Acta Ophthalmol Scand*. 1997;75:325–328.
23. Siggs OM, Souzeau E, Breen J, et al. Autosomal dominant nanophthalmos and high hyperopia associated with a C-terminal frameshift variant in MYRF. *Mol Vis*. 2019;25:527–534.
24. Guo C, Zhao Z, Zhang D, et al. Anterior segment features in nanophthalmos with secondary chronic angle closure glaucoma: an ultrasound biomicroscopy study. *Invest Ophthalmol Vis Sci*. 2019;60:2248–2256.
25. Wu W, Dawson DG, Sugar A, et al. Cataract surgery in patients with nanophthalmos: results and complications. *J Cataract Refract Surg*. 2004;30:584–590.
26. Fujita T, Tsuruga E, Yamanouchi K, Sawa Y, Ishikawa H. Microfibril-associated glycoprotein-1 controls human ciliary zonule development in vitro. *Acta Histochem Cytochem*. 2014;47:11–17.
27. Chen Y, Gao J, Li L, et al. The ciliary muscle and zonules of Zinn modulate lens intracellular hydrostatic pressure through transient receptor potential vanilloid channels. *Invest Ophthalmol Vis Sci*. 2019;60:4416–4424.
28. Nankivil D, Manns F, Arrieta-Quintero E, et al. Effect of anterior zonule transection on the change in lens diameter and power in cynomolgus monkeys during simulated accommodation. *Invest Ophthalmol Vis Sci*. 2009;50:4017–4021.
29. Jones W, Rodriguez J, Bassnett S. Targeted deletion of fibrillin-1 in the mouse eye results in ectopia lentis and other ocular phenotypes associated with Marfan syndrome. *Dis Model Mech*. 2019;12(1):dmm037283.
30. Shi Y, Tu Y, De Maria A, Mecham RP, Bassnett S. Development, composition, and structural arrangements of the ciliary zonule of the mouse. *Invest Ophthalmol Vis Sci*. 2013;54:2504–2515.
31. Calvo J, Boya J. Oxytalan fibres in the rat pineal gland. *J Anat*. 1983;136:363–366.
32. Eckersley A, Mellody KT, Pilkington S, et al. Structural and compositional diversity of fibrillin microfibrils in human tissues. *J Biol Chem*. 2018;293:5117–5133.
33. Hubmacher D, Apte SS. ADAMTS proteins as modulators of microfibril formation and function. *Matrix Biol*. 2015;47:34–43.
34. Inoue T, Ohbayashi T, Fujikawa Y, et al. Latent TGF-β binding protein-2 is essential for the development of ciliary zonule microfibrils. *Hum Mol Genet*. 2014;23:5672–5682.
35. Hanssen E, Franc S, Garrone R. Synthesis and structural organization of zonular fibers during development and aging. *Matrix Biol*. 2001;20:77–85.
36. Judge DP, Biery NJ, Keene DR, et al. Evidence for a critical contribution of haploinsufficiency in the complex pathogenesis of Marfan syndrome. *J Clin Invest*. 2004;114:172–181.
37. Beene LC, Wang LW, Hubmacher D, et al. Nonselective assembly of fibrillin 1 and fibrillin 2 in the rodent ocular zonule and in cultured cells: implications for Marfan syndrome. *Invest Ophthalmol Vis Sci*. 2013;54:8337–8344.
38. Shi Y, Tu Y, Mecham RP, Bassnett S. Ocular phenotype of FBN2-null mice. *Invest Ophthalmol Vis Sci*. 2013;54:7163–7173.
39. Inoue T, Ohbayashi T, Fujikawa Y, et al. Latent TGF-beta binding protein-2 is essential for the development of ciliary zonule microfibrils. *Hum Mol Genet*. 2014;23:5672–5682.
40. Collin GB, Hubmacher D, Charette JR, et al. Disruption of murine ADAMTSL4 results in zonular fiber detachment from the lens and in retinal pigment epithelium dedifferentiation. *Hum Mol Genet*. 2015;24:6958–6974.
41. Mandal MN, Vasireddy V, Reddy GB, et al. CTRP5 is a membrane-associated and secretory protein in the RPE and ciliary body and the S163R mutation of CTRP5 impairs its secretion. *Invest Ophthalmol Vis Sci*. 2006;47:5505–5513.
42. Muhtaseb M, Kalhoro A, Ionides A. A system for preoperative stratification of cataract patients according to risk of intraoperative complications: a prospective analysis of 1441 cases. *Br J Ophthalmol*. 2004;88:1242–1246.

Investigative Ophthalmology & Visual Science